Supporting Information

Positive Modulators of the N-Methyl-D-Aspartate Receptor: Structure-Activity Relationship Study on Steroidal 3-Hemiesters

Barbora Krausova[1], Barbora Slavikova[2], Michaela Nekardova[2,3], Pavla Hubalkova[1,4], Vojtech Vyklicky[1], Hana Chodounska[2], Ladislav Vyklicky[1], Eva Kudova[2,*]

[1]Institute of Physiology of the Czech Academy of Sciences, Videnska 1083, Prague 4, 142 20, Czech Republic
[2]Institute of Organic Chemistry and Biochemistry of the Czech Academy of Sciences, Flemingovo nam. 2, Prague 6, 166 10, Czech Republic
[3]Faculty of Mathematics and Physics, Charles University in Prague, Ke Karlovu 3, Prague 2, 121 16, Czech Republic
[4] Third Faculty of Medicine, Charles University in Prague, Ruska 87, Prague 10, 100 00, Czech Republic

Table of Content

Table S1. Summary of computational values of physicochemical properties of compounds **1-24**.

	ΔG_{solv} [kcal/mol] - transfer from					
	vacuum to water		*n*-octanol to water			
Compound	neutral	charged	neutral	charged	**LogP**	**LogD**
1 (PES)	-21.10	-75.74	1.76	-5.67	**2.02**	**1.26**
2	-17.62	-79.36	3.40	-4.88	**3.49**	**0.71**
3	-20.10	-81.91	3.79	-5.33	**3.81**	**0.84**
4	-20.30	-85.84	4.17	-5.56	**4.27**	**0.73**
5	-21.68	-88.61	4.42	-5.21	**4.41**	**1.29**
6	-21.10	-88.10	5.18	-4.35	**4.97**	**1.75**
7	-21.09	-88.77	5.87	-4.02	**5.46**	**2.09**
8	-20.70	-88.52	6.54	-3.24	**6.00**	**2.64**
9	-12.15	-75.10	6.43	-2.78	**5.29**	**2.02**
10	-12.51	-79.10	6.82	-3.03	**5.74**	**1.91**
11	-13.86	-81.37	7.06	-2.62	**6.14**	**2.47**
12	-13.25	-80.81	7.87	-1.76	**6.44**	**2.92**
13	-13.23	-81.47	8.51	-1.44	**6.76**	**3.27**
14	-12.73	-75.49	5.45	-3.60	**4.64**	**1.28**
15	-12.92	-79.73	5.95	-3.96	**4.91**	**1.18**
16	-14.35	-81.93	6.15	-3.57	**5.22**	**1.74**
17	-13.66	-81.30	6.95	-2.70	**5.81**	**2.19**
18	-13.69	-81.88	7.62	-2.26	**6.29**	**2.54**
19	-22.65	-89.39	3.52	-6.08	**3.73**	**1.07**
20	-22.03	-88.88	4.32	-5.21	**4.32**	**1.53**
21	-22.02	-89.78	5.01	-4.91	**4.81**	**1.87**
22	-21.57	-89.57	5.72	-4.23	**5.25**	**2.42**
23	-21.45	-89.76	6.31	-3.59	**5.26**	**3.00**
24	-26.87	-89.56	5.77	-2.82	**5.40**	**3.94**

Preparation of structures.

The studied compounds were manually built in PyMOL (version 1.5.0.4.)[1] using the geometry of the molecule taken from the crystal structure (3CAV PDB code),[2] and were relaxed by the RI-DFT/B-LYP/SVP method with the program Turbomole (version 6.1).[3] The empirical dispersion correction (D)[4] and COSMO continuum solvation model[5] were applied on the gradient optimization. The most stable local minima of the compounds were generated by the molecular dynamics simulation with a general AMBER empirical force field (the simulation was run for 30 ns; the constant temperature was 400 K).[6] The package AMBER 14 MD was used.[7] The partial charges of the molecules were calculated using the RESP procedure[8] at the HF/6-31G* level. The resulting geometries were minimized by the RI-DFT-D/B-LYP/SVP//COSMO method and their single-point energies (SP) were calculated at the RI-DFT-D3/B-LYP/TZVPP//COSMO level.[9] The chosen structures were re-optimized by the RI-DFT-D3/B-LYP/TZVPP//COSMO method and their SP were calculated at the same level of accuracy.

Computational methods.

The solvation free energy (ΔG_{solv}) of the compounds was calculated in the SMD continuum solvation model[10] (the transfer from vacuum to water and from *n*-octanol to water) at the HF/6-31G* level with the program Gaussian (version 09).[11] In this method, the single-point energies were computed with an identical molecular geometry for both the transfer from vacuum to water and from *n*-octanol to water. The partition coefficient (P) is defined as the ratio of concentrations of a neutral solute in *n*-octanol and water, and it represents the solute lipophilicity. It is usually reported as the common logarithm:

$$logP = log\left(c_{neutral,octanol}/c_{neutral,water}\right)$$

The calculated logP was obtained via the equation $logP = \Delta G_{ow}/\left(-RTln(10)\right)$, where ΔG_{ow} is the transfer free energy, R is the molar gas constant and T is temperature (298.15 K).[12]

The ΔG_{ow} was calculated on the basis of the change in the molecular conformation related to the transfer between *n*-octanol and water. The compounds were optimized at the M06-2X/6-31G* level in SMD with Gaussian, and ΔG_{ow} was expressed as the difference between the total energies in water and in *n*-octanol, because this energy includes the internal energy of the molecule.[12a]

The distribution-coefficient (D), which is also presented as a common logarithm, takes into account both the neutral and ionized form of the solute in both phases and is used for estimating the lipophilicity of ionizable species.[13]

$$logD = log\left(\left(c_{ionized,octanol} + c_{neutral,octanol}\right)/\left(c_{ionized,water} + c_{neutral,water}\right)\right)$$

The logD values were predicted at pH = 7.4, which is the physiological pH of blood serum, using the program MarvinSketch.[14]

REFERENCES

1. *The PyMOL Molecular Graphics System*, version 1.5.0.4; Schrödinger: LLC.
2. Faucher, F.; Cantin, L.; Luu-The, V.; Labrie, F.; Breton, R. The crystal structure of human delta4-3-ketosteroid 5beta-reductase defines the functional role of the residues of the catalytic tetrad in the steroid double bond reduction mechanism. *Biochemistry* **2008**, *47 (32)*, 8261–8270.
3. Ahlrichs, R. B., M.; Haser, M.; Horn, H.; Kolmel, C. Electronic structure calculations on workstation computers: The program system Turbomole. *Chem. Phys. Lett.* **1989**, *162*, 165–169.
4. Jurecka, P.; Cerny, J.; Hobza, P.; Salahub, D. R. Density functional theory augmented with an empirical dispersion term. Interaction energies and geometries of 80 noncovalent complexes compared with ab initio quantum mechanics calculations. *J. Comput. Chem.* **2007**, *28 (2)*, 555-569.
5. Klamt, A. S., G., COSMO: A new approach to dielectric screening in solvents with explicit expressions for the screening energy and its gradient. *J. Chem. Soc., Perkin Trans 2* **1993**, *5*, 799–805.
6. Wang, J.; Wolf, R. M.; Caldwell, J. W.; Kollman, P. A.; Case, D. A. Development and testing of a general amber force field. *J. Comput. Chem.* **2004**, *25 (9)*, 1157–1174.
7. Case, D. A. B., V.; Berryman, J. T.; Betz, R. M.; Cai, Q.; Cerutti, D. S.; Cheatham, I. T. E.; Darden, T. A.; Duke, R. E.; Gohlke, H.; Goetz, A. W.; Gusarov, S.; Homeyer, N.; Janowski, P.; Kaus, J.; Kolossváry, I.; Kovalenko, A.; Lee, T. S.; LeGrand, S.; Luchko, T.; Luo, R.; Madej, B.; Merz, K. M.; Paesani, F.; Roe, D. R.; Roitberg, A.; Sagui, C.; Salomon-Ferrer, R.; Seabra, G.; Simmerling, C. L.; Smith, W.; Swails, J.; Walker, R. C.; Wang, J.; Wolf, R. M.; Wu, X.; Kollman, P. A. *AMBER 14.*, University of California: San Francisco, **2014**.
8. Bayly, C. I. C., P.; Cornell, W. D.; Kollman, P. A. A well-behaved electrostatic potential based method using charge restraints for deriving atomic charges - the RESP Model. *J. Phys. Chem.* **1993**, *97*, 10269–10280.
9. Grimme, S.; Antony, J.; Ehrlich, S.; Krieg, H. A consistent and accurate ab initio parametrization of density functional dispersion correction (DFT-D) for the 94 elements H-Pu. *J. Chem. Phys.* **2010**, *132 (15)*, 154104.
10. Marenich, A. V.; Cramer, C. J.; Truhlar, D. G. Universal solvation model based on solute electron density and on a continuum model of the solvent defined by the bulk dielectric constant and atomic surface tensions. *J. Phys. Chem. B* **2009**, *113 (18)*, 6378–6396.
11. Frisch, M. J. T., G. W.; Schlegel, H. B.; Scuseria, G. E.; Robb, M. A.; Cheeseman, J. R.; Scalmani, G.; Barone, V.; Mennucci, B.; Petersson, G. A.; Nakatsuji, H.; Caricato, M.; Li, X.; Hratchian, H. P.; Izmaylov, A. F.; Bloino, J.; Zheng, G.; Sonnenberg, J. L.; Hada, M.; Ehara, M.; Toyota, K.; Fukuda, R.; Hasegawa, J.; Ishida, M.; Nakajima, T.; Honda, Y.; Kitao, O.; Nakai, H.; Vreven, T.; Montgomery, J. A., Jr.; Peralta, J. E.; Ogliaro, F.; Bearpark, M.; Heyd, J. J.; Brothers, E.; Kudin, K. N.; Staroverov, V. N.; Kobayashi, R.; Normand, J.; Raghavachari, K.; Rendell, A.; Burant, J. C.; Iyengar, S. S.; Tomasi, J.; Cossi, M.; Rega, N.; Millam, N. J.; Klene, M.; Knox, J. E.; Cross, J. B.; Bakken, V.; Adamo, C.; Jaramillo, J.; Gomperts, R.; Stratmann, R. E.; Yazyev, O.; Austin, A. J.; Cammi, R.; Pomelli, C.; Ochterski, J. W.; Martin, R. L.; Morokuma, K.; Zakrzewski, V. G.; Voth, G. A.; Salvador, P.; Dannenberg, J. J.; Dapprich, S.; Daniels, A. D.; Farkas, Ö.; Foresman, J. B.; Ortiz, J. V.; Cioslowski, J.; Fox, D. J. *Gaussian 09*, Gaussian Inc.: Wallingford, CT, **2009**.
12. (a) Kolar, M.; Fanfrlik, J.; Lepsik, M.; Forti, F.; Luque, F. J.; Hobza, P. Assessing the accuracy and performance of implicit solvent models for drug molecules: conformational

ensemble approaches. *J. Phys. Chem. B* **2013**, *117 (19)*, 5950–5962; (b) Bannan, C. C.; Calabro, G.; Kyu, D. Y.; Mobley, D. L. Calculating partition coefficients of small molecules in octanol/water and cyclohexane/water. *J. Chem. Theory Comput.* **2016**, *12 (8)*, 4015–4024.
13. Kah, M.; Brown, C. D. LogD: lipophilicity for ionisable compounds. *Chemosphere* **2008**, *72 (10)*, 1401–1408.
14. Marvin version 15.1.19; ChemAxon: http://www.chemaxon.com, **2015**.

Purity of compounds.

The purity of compounds was monitored over time using an Agilent 6230 TOF LC/MS. Samples were separated on a Waters ACQUITY UPLC CSH Phenyl-Hexyl (100×2.1, 130Å, 1.7 µm) at a flow rate 0.3 ml/min. The concentration of mobile phase B (0.1% FA in acetonitrile) was gradually increased from 15 to 100 % in mobile phase A (0.1% FA in water) over 5.5 min. The mass spectrometry instrument was operated in a negative ion mode with a voltage of +3.00 kV applied to the capillary. The temperature, the flow rate of the nitrogen drying gas, the pressure of the nitrogen nebulizing gas, the temperature, and the flow rate of the sheath gas were set at 325°C, 10 l/min, 40 psi, 390°C, and 11 l/min, respectively.

Compound 2:

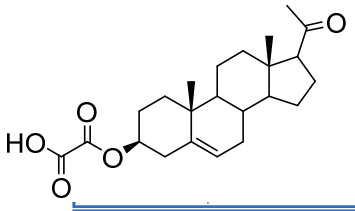
HO
O
O
O
O

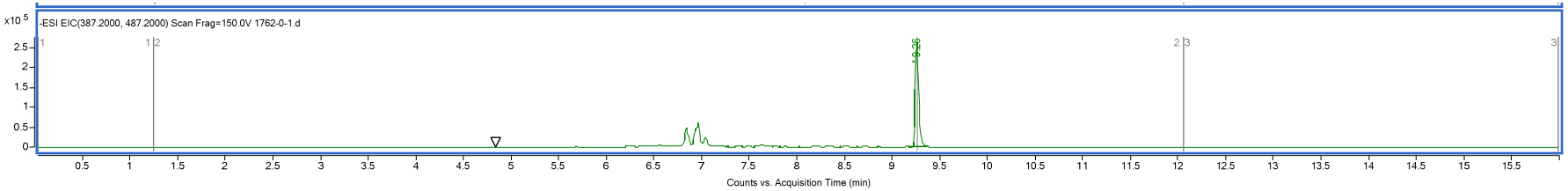
x10 5
-ESI EIC(387.2000, 487.2000) Scan Frag=150.0V 1762-0-1.d
9.26
Counts vs. Acquisition Time (min)

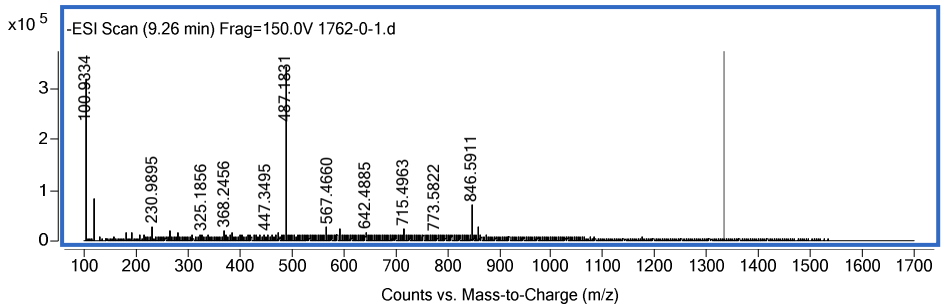
x10 5
-ESI Scan (9.26 min) Frag=150.0V 1762-0-1.d
100.9334
230.9895
325.1856
368.2456
447.3495
487.1831
567.4660
642.4885
715.4963
773.5822
846.5911
Counts vs. Mass-to-Charge (m/z)

Compound 3:

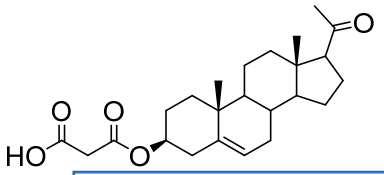
HO
O
O
O
O

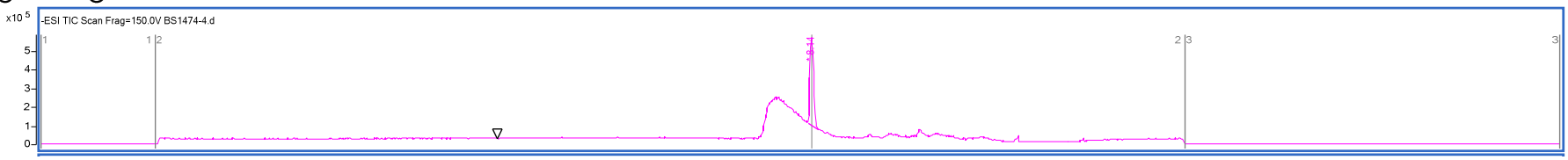
x10 5
-ESI TIC Scan Frag=150.0V BS1474-4.d
1
1 2
2 3
3
5
4
3
2
1
0

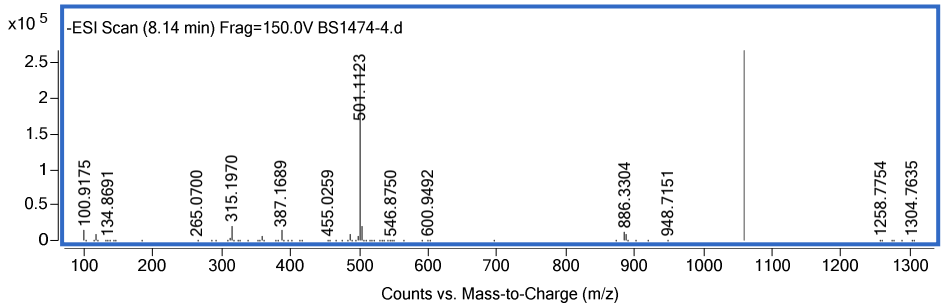
x10 5
-ESI Scan (8.14 min) Frag=150.0V BS1474-4.d
2.5
2
1.5
1
0.5
0
100.9175
134.8691
265.0700
315.1970
387.1689
455.0259
501.1123
546.8750
600.9492
886.3304
948.7151
1258.7754
1304.7635
100
200
300
400
500
600
700
800
900
1000
1100
1200
1300
Counts vs. Mass-to-Charge (m/z)

Compound 4:

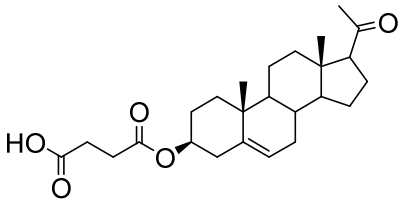
HO
O
O
O
O

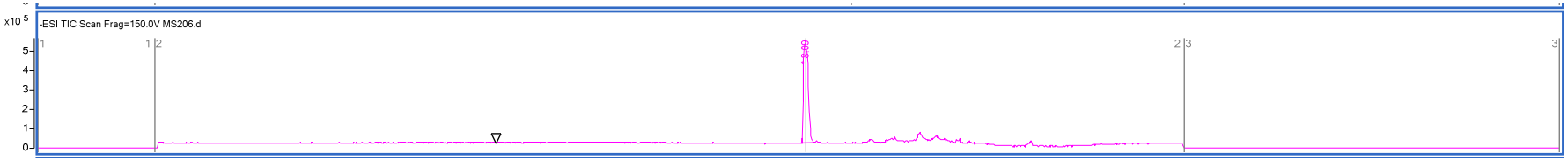
x10 5
-ESI TIC Scan Frag=150.0V MS206.d
5
4
3
2
1
0

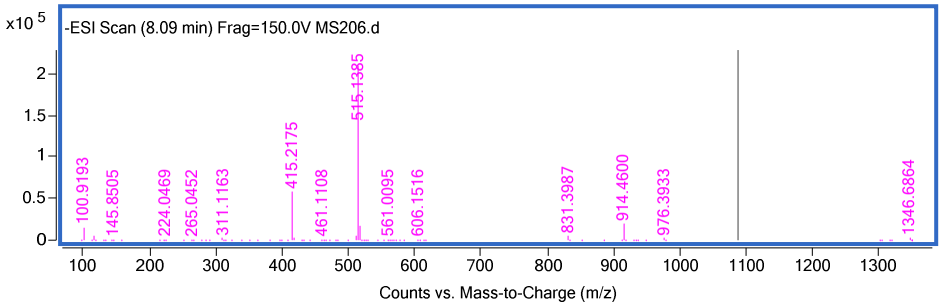
x10 5
-ESI Scan (8.09 min) Frag=150.0V MS206.d
2
1.5
1
0.5
0
100.9193
145.8505
224.0469
265.0452
311.1163
415.2175
461.1108
515.1385
561.0095
606.1516
831.3987
914.4600
976.3933
1346.6864
100
200
300
400
500
600
700
800
900
1000
1100
1200
1300
Counts vs. Mass-to-Charge (m/z)

Compound 5:

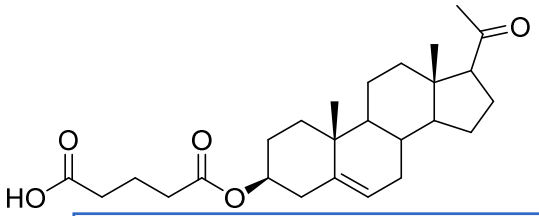
HO
O
O
O
O

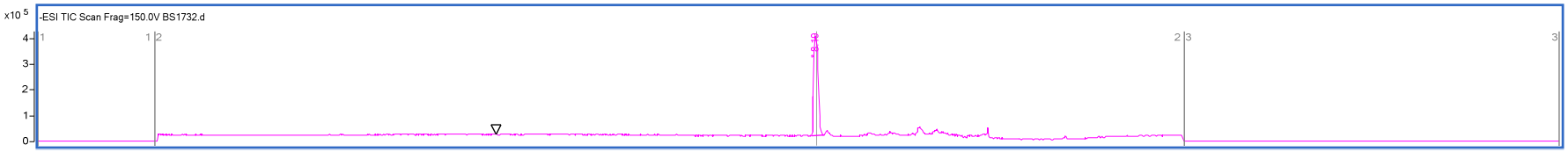
x10 5
-ESI TIC Scan Frag=150.0V BS1732.d
4
3
2
1
0
1
1 2
2 3
3

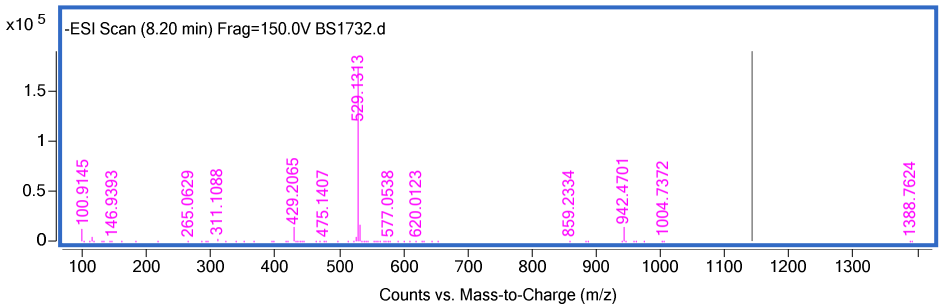
x10 5
-ESI Scan (8.20 min) Frag=150.0V BS1732.d
1.5
1
0.5
0
100.9145
146.9393
265.0629
311.1088
429.2065
475.1407
529.1313
577.0538
620.0123
859.2334
942.4701
1004.7372
1388.7624
100
200
300
400
500
600
700
800
900
1000
1100
1200
1300
Counts vs. Mass-to-Charge (m/z)

Compound 6:

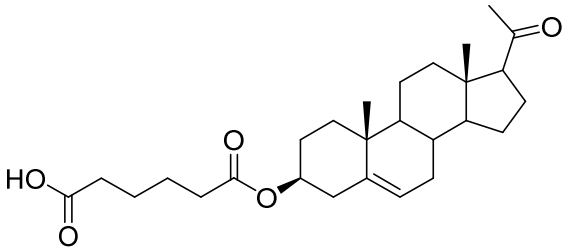
HO
O
O
O
O

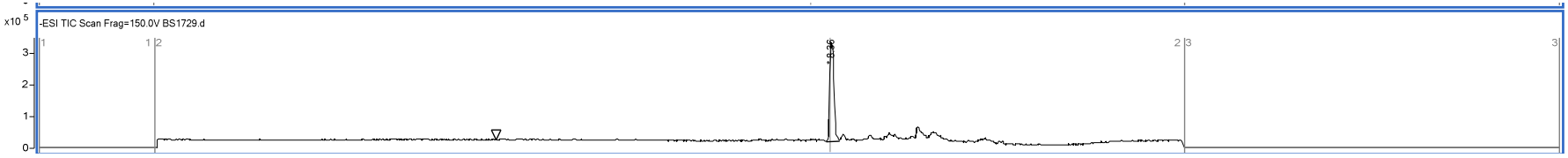
x10 5
-ESI TIC Scan Frag=150.0V BS1729.d
3
2
1
0

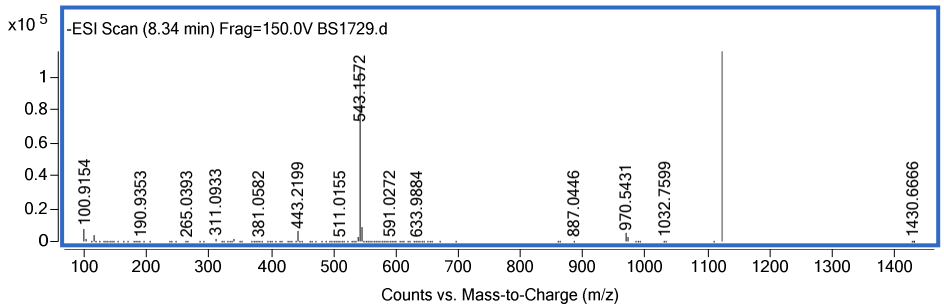
x10 5
-ESI Scan (8.34 min) Frag=150.0V BS1729.d
1
0.8
0.6
0.4
0.2
0
100.9154
190.9353
265.0393
311.0933
381.0582
443.2199
511.0155
543.1572
591.0272
633.9884
887.0446
970.5431
1032.7599
1430.6666
100
200
300
400
500
600
700
800
900
1000
1100
1200
1300
1400
Counts vs. Mass-to-Charge (m/z)

Compound 7:

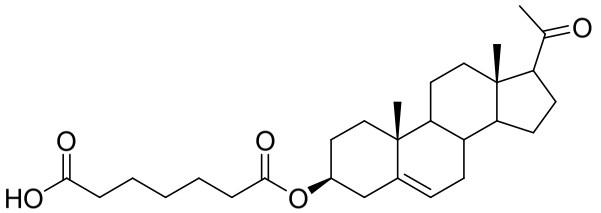
HO
O
O
O
O

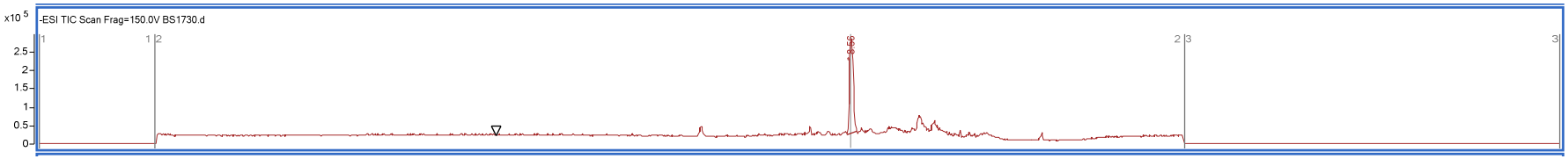
x10 5
-ESI TIC Scan Frag=150.0V BS1730.d
2.5
2
1.5
1
0.5
0

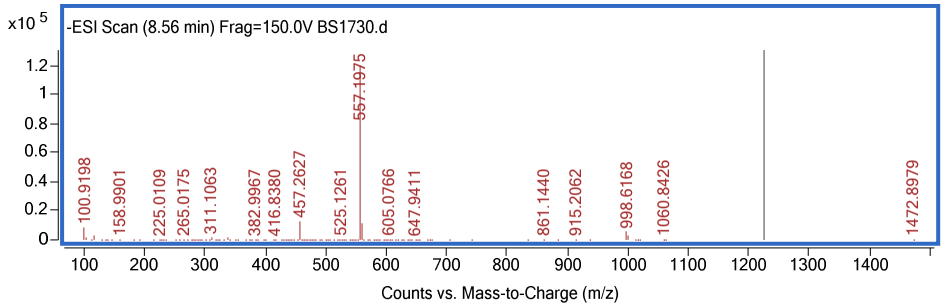
x10 5
-ESI Scan (8.56 min) Frag=150.0V BS1730.d
1.2
1
0.8
0.6
0.4
0.2
0
100.9198
158.9901
225.0109
265.0175
311.1063
382.9967
416.8380
457.2627
525.1261
557.1975
605.0766
647.9411
861.1440
915.2062
998.6168
1060.8426
1472.8979
100
200
300
400
500
600
700
800
900
1000
1100
1200
1300
1400
Counts vs. Mass-to-Charge (m/z)

Compound 8:

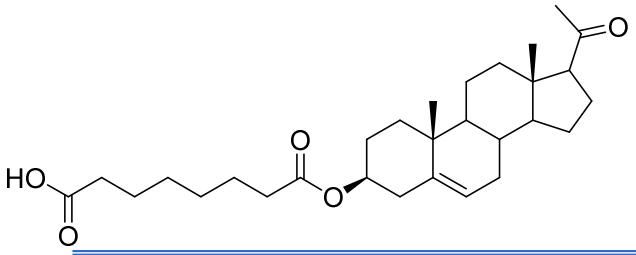
HO
O
O
O
O

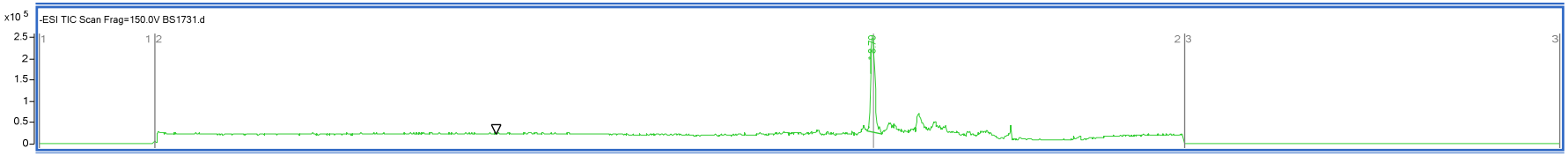
x10 5
-ESI TIC Scan Frag=150.0V BS1731.d
2.5
2
1.5
1
0.5
0
1
1 2
2 3
3

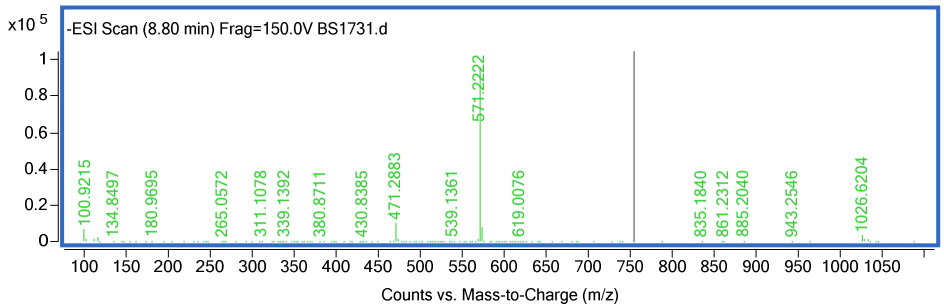
x10 5
-ESI Scan (8.80 min) Frag=150.0V BS1731.d
1
0.8
0.6
0.4
0.2
0
100.9215
134.8497
180.9695
265.0572
311.1078
339.1392
380.8711
430.8385
471.2883
539.1361
571.2222
619.0076
835.1840
861.2312
885.2040
943.2546
1026.6204
100 150 200 250 300 350 400 450 500 550 600 650 700 750 800 850 900 950 1000 1050
Counts vs. Mass-to-Charge (m/z)

Compound 9:

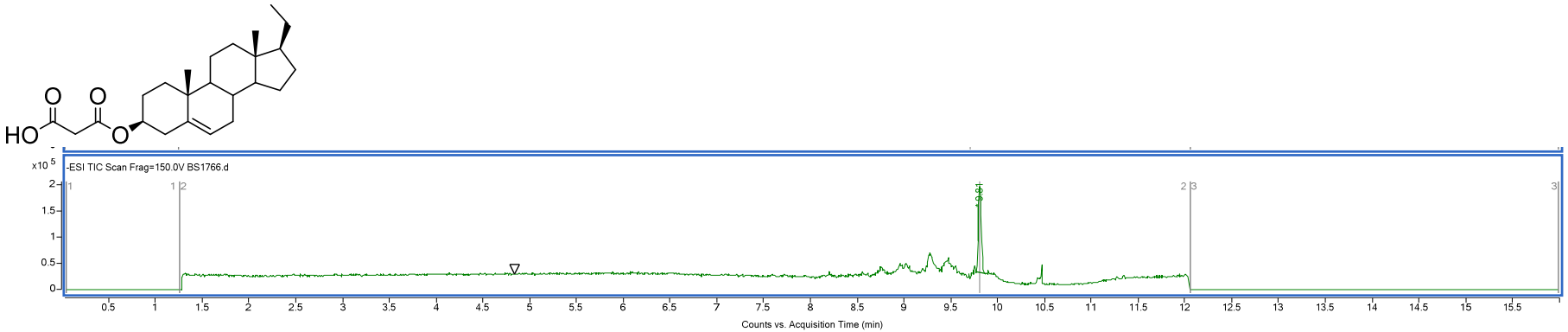
HO
O
O
O
x10 5
-ESI TIC Scan Frag=150.0V BS1766.d
9.81
Counts vs. Acquisition Time (min)

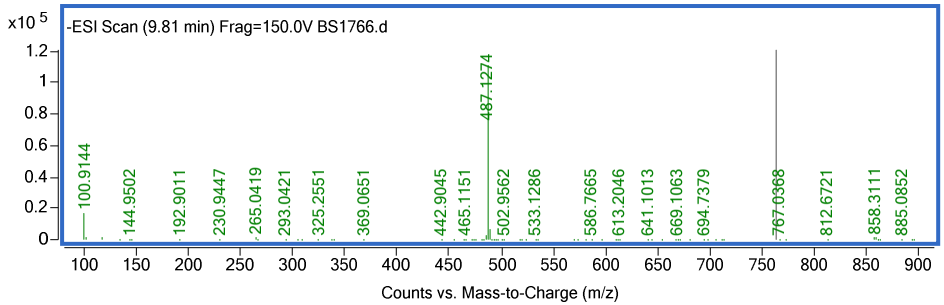
x10 5
-ESI Scan (9.81 min) Frag=150.0V BS1766.d
100.9144
144.9502
192.9011
230.9447
265.0419
293.0421
325.2551
369.0651
442.9045
465.1151
487.1274
502.9562
533.1286
586.7665
613.2046
641.1013
669.1063
694.7379
767.0368
812.6721
858.3111
885.0852
Counts vs. Mass-to-Charge (m/z)

Compound 10:

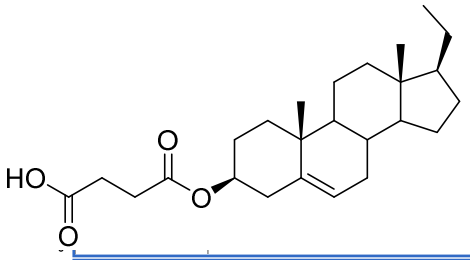
HO
O
O
O

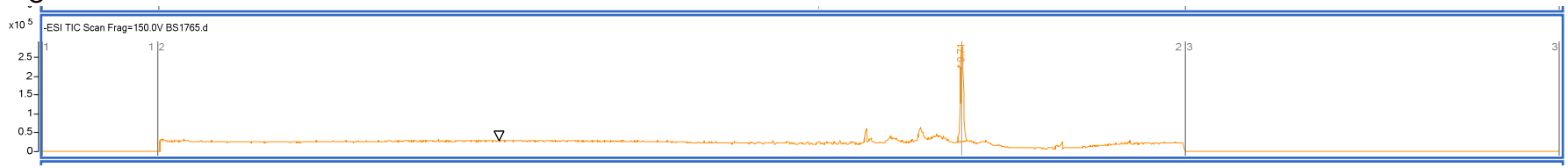
x10 5
-ESI TIC Scan Frag=150.0V BS1765.d
2.5
2
1.5
1
0.5
0
9.71

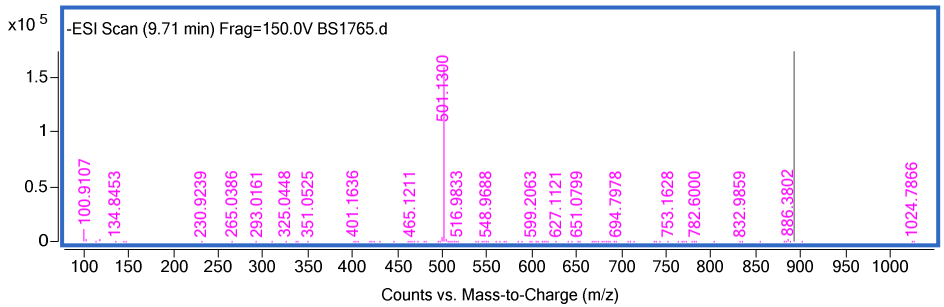
x10 5
-ESI Scan (9.71 min) Frag=150.0V BS1765.d
1.5
1
0.5
0
100.9107
134.8453
230.9239
265.0386
293.0161
325.0448
351.0525
401.1636
465.1211
501.1300
516.9833
548.9688
599.2063
627.1121
651.0799
694.7978
753.1628
782.6000
832.9859
886.3802
1024.7866
100 150 200 250 300 350 400 450 500 550 600 650 700 750 800 850 900 950 1000
Counts vs. Mass-to-Charge (m/z)

Compound 11:

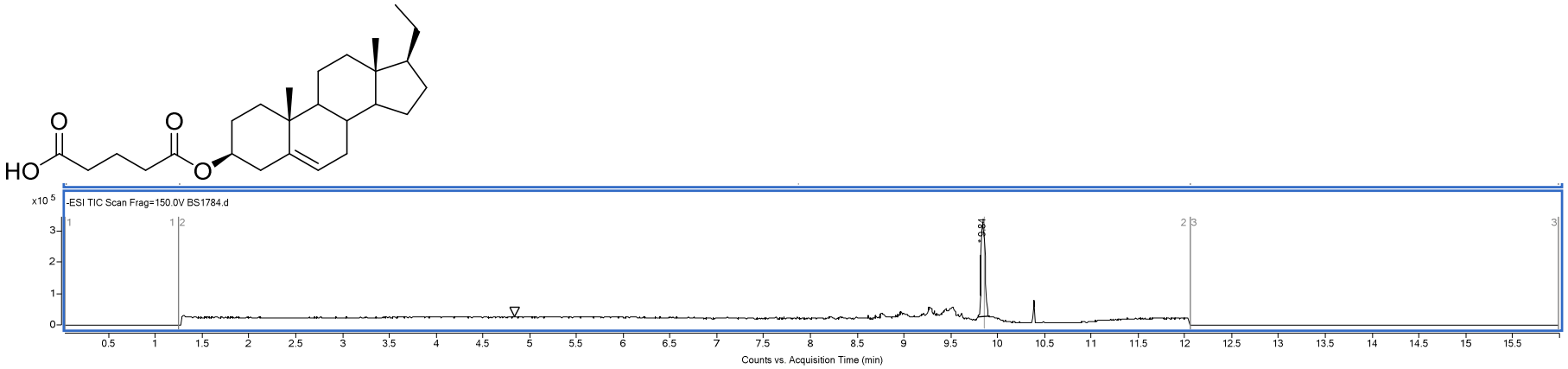
HO
O
O
O
x10 5
-ESI TIC Scan Frag=150.0V BS1784.d
Counts vs. Acquisition Time (min)

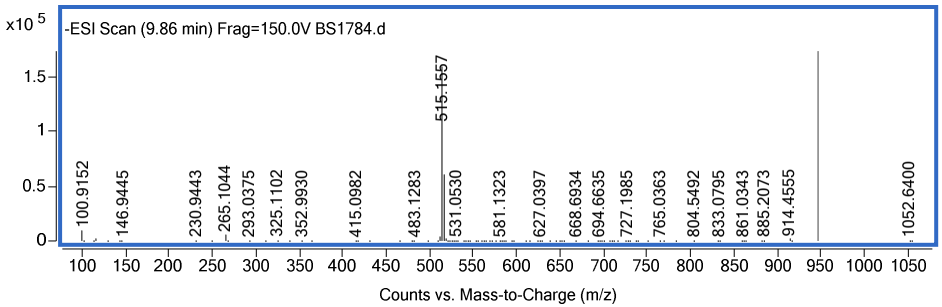
x10 5
-ESI Scan (9.86 min) Frag=150.0V BS1784.d
100.9152
146.9445
230.9443
265.1044
293.0375
325.1102
352.9930
415.0982
483.1283
515.1557
531.0530
581.1323
627.0397
668.6934
694.6635
727.1985
765.0363
804.5492
833.0795
861.0343
885.2073
914.4555
1052.6400
Counts vs. Mass-to-Charge (m/z)

Compound 12:

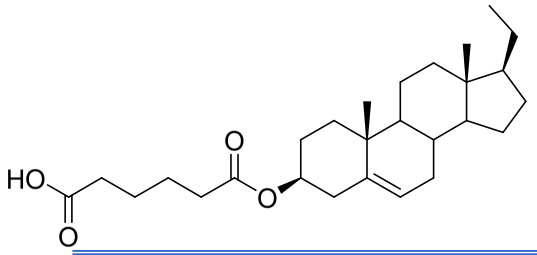
HO
O
O
O

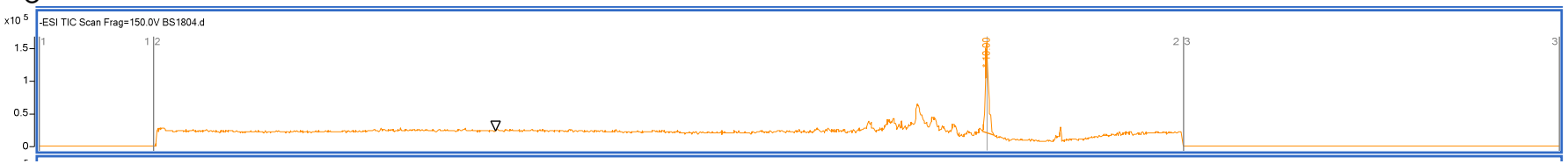
x10 5
-ESI TIC Scan Frag=150.0V BS1804.d
1.5
1
0.5
0

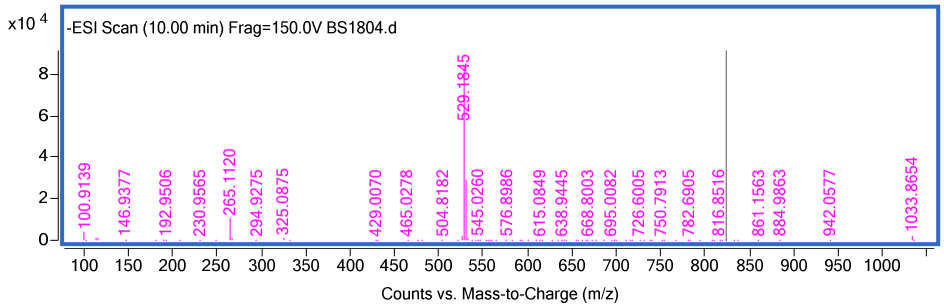
x10 4
-ESI Scan (10.00 min) Frag=150.0V BS1804.d
8
6
4
2
0
100.9139
146.9377
192.9506
230.9565
265.1120
294.9275
325.0875
429.0070
465.0278
504.8182
529.1845
545.0260
576.8986
615.0849
638.9445
668.8003
695.0082
726.6005
750.7913
782.6905
816.8516
861.1563
884.9863
942.0577
1033.8654
100 150 200 250 300 350 400 450 500 550 600 650 700 750 800 850 900 950 1000
Counts vs. Mass-to-Charge (m/z)

Compound 13:

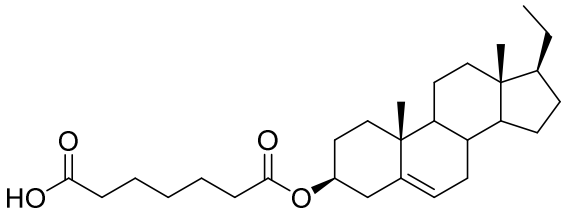
HO
O
O
O

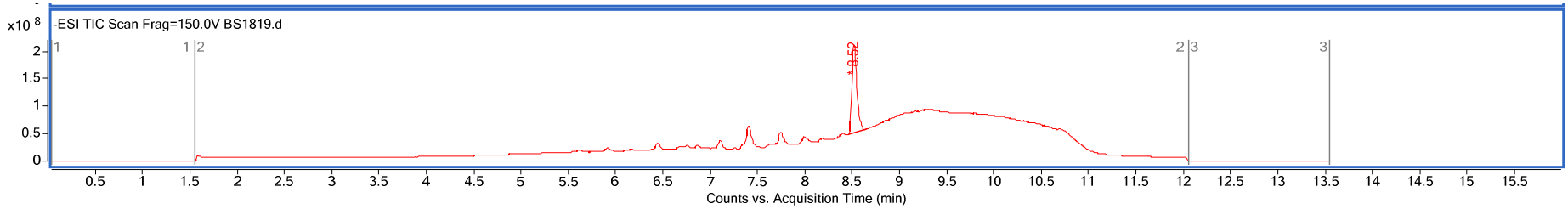
x10 8
-ESI TIC Scan Frag=150.0V BS1819.d
1
1 2
8.52
2 3
3
2
1.5
1
0.5
0
0.5 1 1.5 2 2.5 3 3.5 4 4.5 5 5.5 6 6.5 7 7.5 8 8.5 9 9.5 10 10.5 11 11.5 12 12.5 13 13.5 14 14.5 15 15.5
Counts vs. Acquisition Time (min)

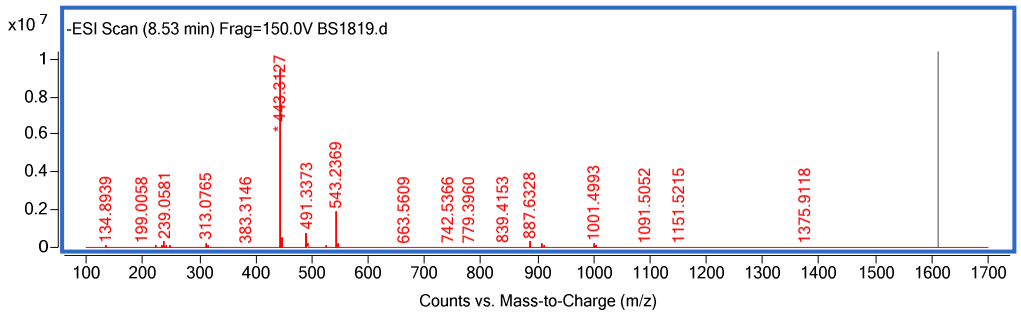
x10 7
-ESI Scan (8.53 min) Frag=150.0V BS1819.d
443.3127
134.8939
199.0058
239.0581
313.0765
383.3146
491.3373
543.2369
663.5609
742.5366
779.3960
839.4153
887.6328
1001.4993
1091.5052
1151.5215
1375.9118
1
0.8
0.6
0.4
0.2
0
100 200 300 400 500 600 700 800 900 1000 1100 1200 1300 1400 1500 1600 1700
Counts vs. Mass-to-Charge (m/z)

Compound 14:

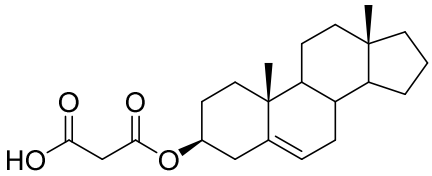
O
O
HO
O

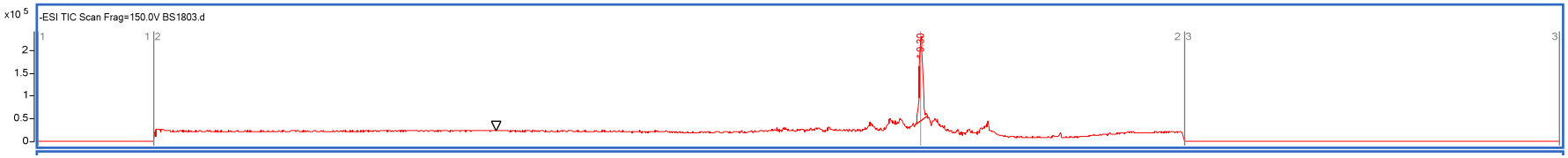
x10 5
-ESI TIC Scan Frag=150.0V BS1803.d
2
1.5
1
0.5
0

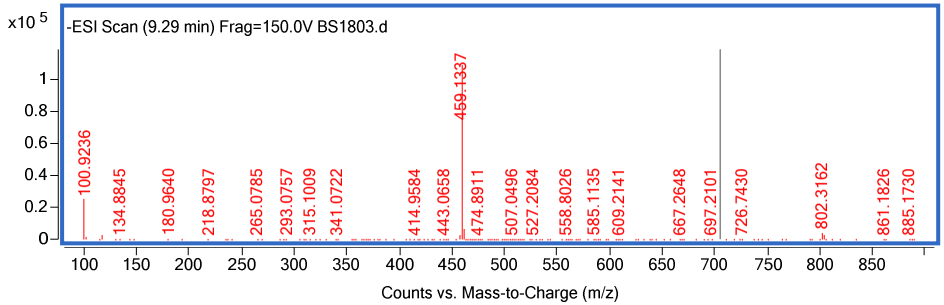
x10 5
-ESI Scan (9.29 min) Frag=150.0V BS1803.d
1
0.8
0.6
0.4
0.2
0
100.9236
134.8845
180.9640
218.8797
265.0785
293.0757
315.1009
341.0722
414.9584
443.0658
459.1337
474.8911
507.0496
527.2084
558.8026
585.1135
609.2141
667.2648
697.2101
726.7430
802.3162
861.1826
885.1730
100
150
200
250
300
350
400
450
500
550
600
650
700
750
800
850
Counts vs. Mass-to-Charge (m/z)

Compound 15:

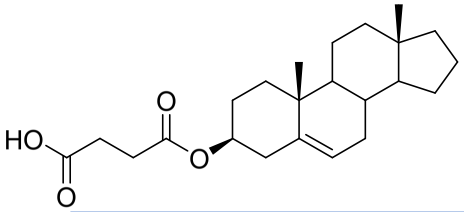
HO
O
O
O

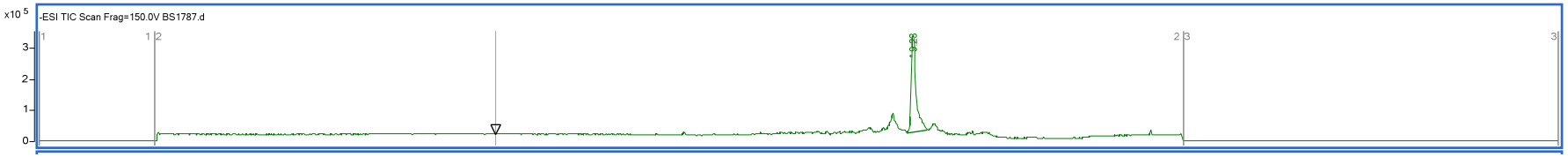
x10 5
-ESI TIC Scan Frag=150.0V BS1787.d
3
2
1
0

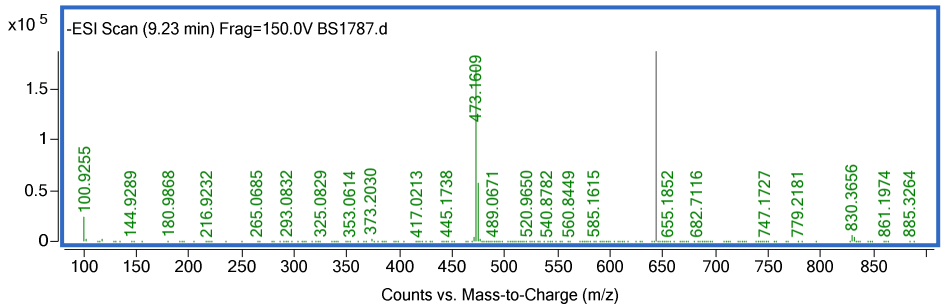
x10 5
-ESI Scan (9.23 min) Frag=150.0V BS1787.d
1.5
1
0.5
0
100.9255
144.9289
180.9868
216.9232
265.0685
293.0832
325.0829
353.0614
373.2030
417.0213
445.1738
473.1609
489.0671
520.9650
540.8782
560.8449
585.1615
655.1852
682.7116
747.1727
779.2181
830.3656
861.1974
885.3264
100
150
200
250
300
350
400
450
500
550
600
650
700
750
800
850
Counts vs. Mass-to-Charge (m/z)

Compound 16:

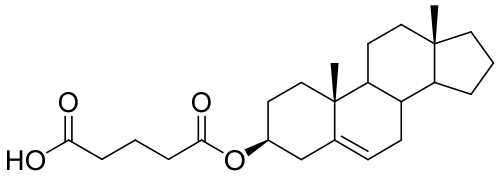
O
O
HO
O

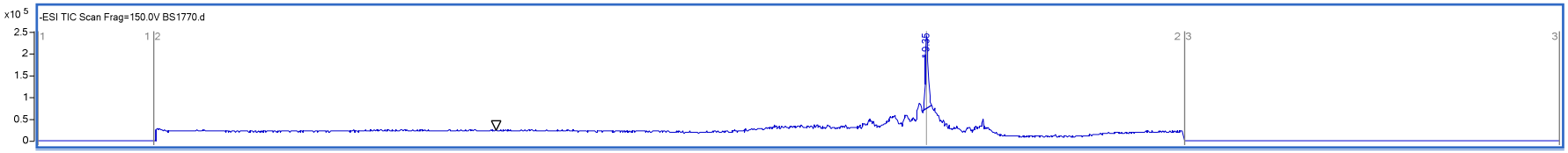
x10 5
-ESI TIC Scan Frag=150.0V BS1770.d
2.5
2
1.5
1
0.5
0
1
1 2
9.35
2 3
3

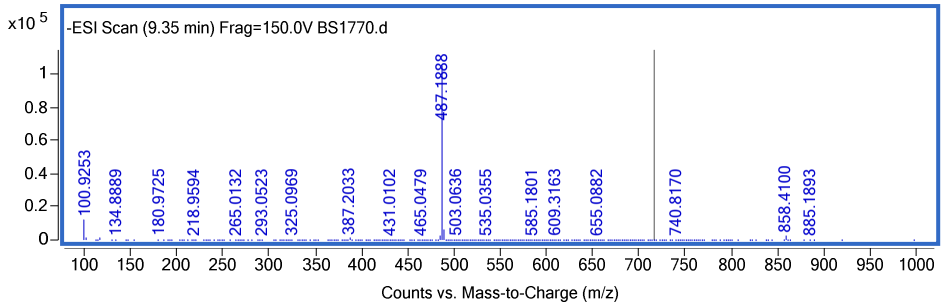
x10 5
-ESI Scan (9.35 min) Frag=150.0V BS1770.d
1
0.8
0.6
0.4
0.2
0
100.9253
134.8889
180.9725
218.9594
265.0132
293.0523
325.0969
387.2033
431.0102
465.0479
487.1888
503.0636
535.0355
585.1801
609.3163
655.0882
740.8170
858.4100
885.1893
100 150 200 250 300 350 400 450 500 550 600 650 700 750 800 850 900 950 1000
Counts vs. Mass-to-Charge (m/z)

Compound 17:

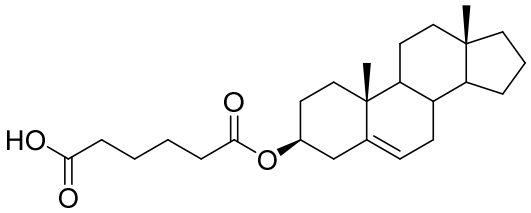
HO
O
O
O

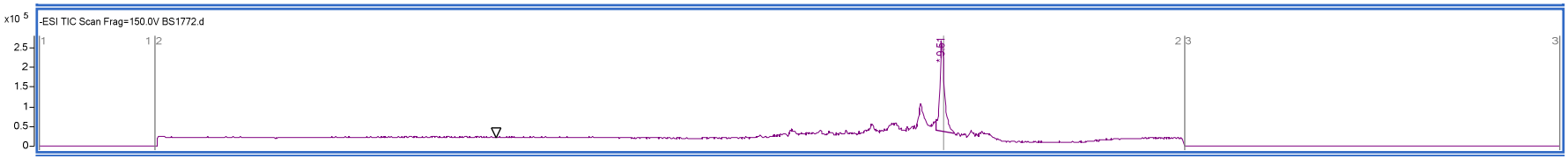
x10 5
-ESI TIC Scan Frag=150.0V BS1772.d
2.5
2
1.5
1
0.5
0
1
2
3
9.51

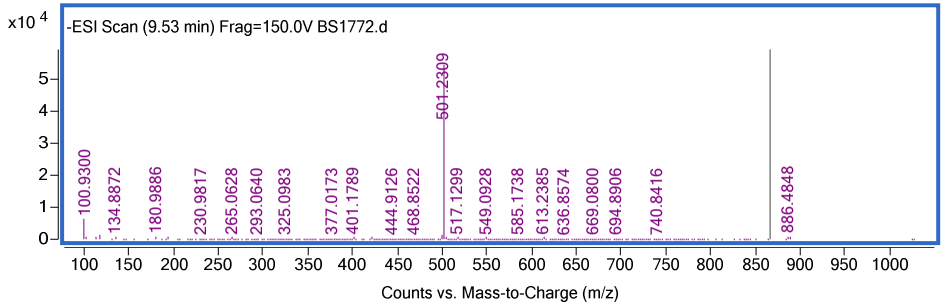
x10 4
-ESI Scan (9.53 min) Frag=150.0V BS1772.d
5
4
3
2
1
0
100.9300
134.8872
180.9886
230.9817
265.0628
293.0640
325.0983
377.0173
401.1789
444.9126
468.8522
501.2309
517.1299
549.0928
585.1738
613.2385
636.8574
669.0800
694.8906
740.8416
886.4848
100
150
200
250
300
350
400
450
500
550
600
650
700
750
800
850
900
950
1000
Counts vs. Mass-to-Charge (m/z)

Compound 18:

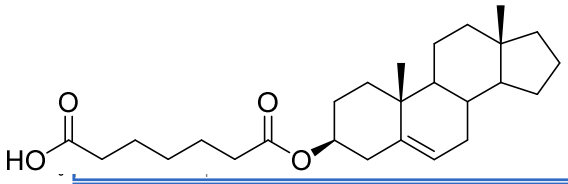
HO
O
O
O

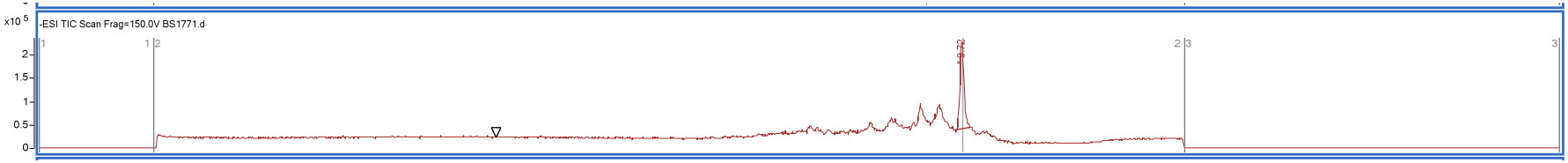
x10 5
-ESI TIC Scan Frag=150.0V BS1771.d
2
1.5
1
0.5
0

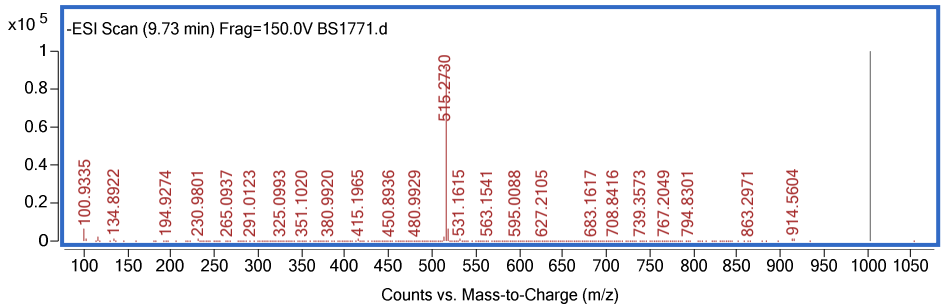
x10 5
-ESI Scan (9.73 min) Frag=150.0V BS1771.d
1
0.8
0.6
0.4
0.2
0
615.2730
100.9335
134.8922
194.9274
230.9801
265.0937
291.0123
325.0993
351.1020
380.9920
415.1965
450.8936
480.9929
531.1615
563.1541
595.0088
627.2105
683.1617
708.8416
739.3573
767.2049
794.8301
863.2971
914.5604
100 150 200 250 300 350 400 450 500 550 600 650 700 750 800 850 900 950 1000 1050
Counts vs. Mass-to-Charge (m/z)

Compound 19:

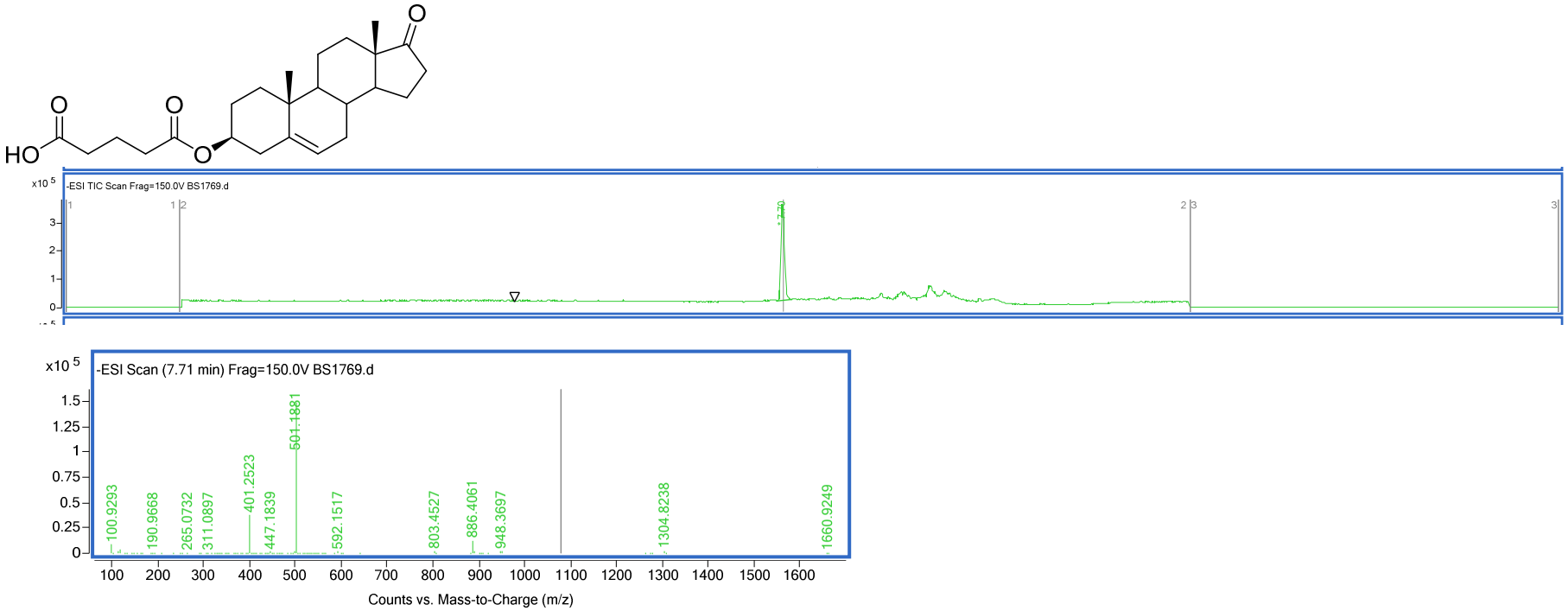
HO
O
O
O
x10 5
-ESI TIC Scan Frag=150.0V BS1769.d
x10 5
-ESI Scan (7.71 min) Frag=150.0V BS1769.d
100.9293
190.9668
265.0732
311.0897
401.2523
447.1839
501.1881
592.1517
803.4527
886.4061
948.3697
1304.8238
1660.9249
Counts vs. Mass-to-Charge (m/z)

Compound 20:

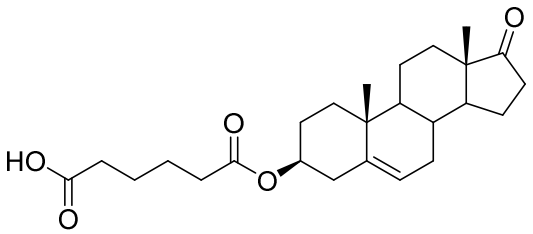
HO
O
O
O
O

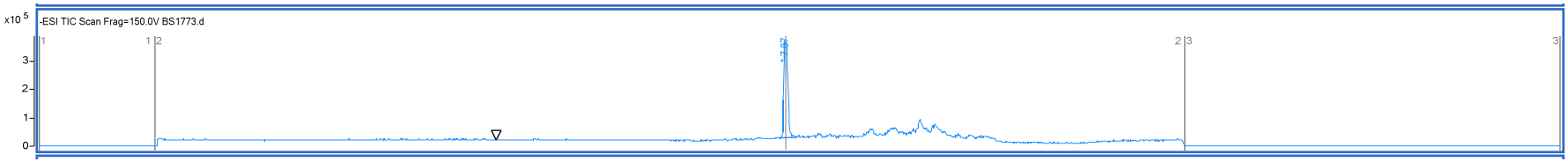
x10 5
-ESI TIC Scan Frag=150.0V BS1773.d
3
2
1
0

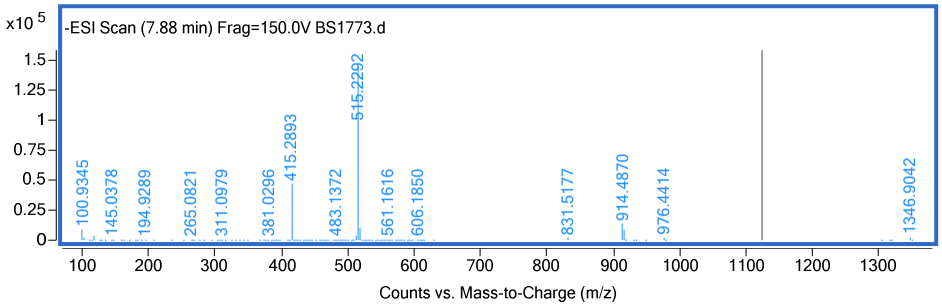
x10 5
-ESI Scan (7.88 min) Frag=150.0V BS1773.d
1.5
1.25
1
0.75
0.5
0.25
0
100.9345
145.0378
194.9289
265.0821
311.0979
381.0296
415.2893
483.1372
515.2292
561.1616
606.1850
831.5177
914.4870
976.4414
1346.9042
100
200
300
400
500
600
700
800
900
1000
1100
1200
1300
Counts vs. Mass-to-Charge (m/z)

Compound 21:

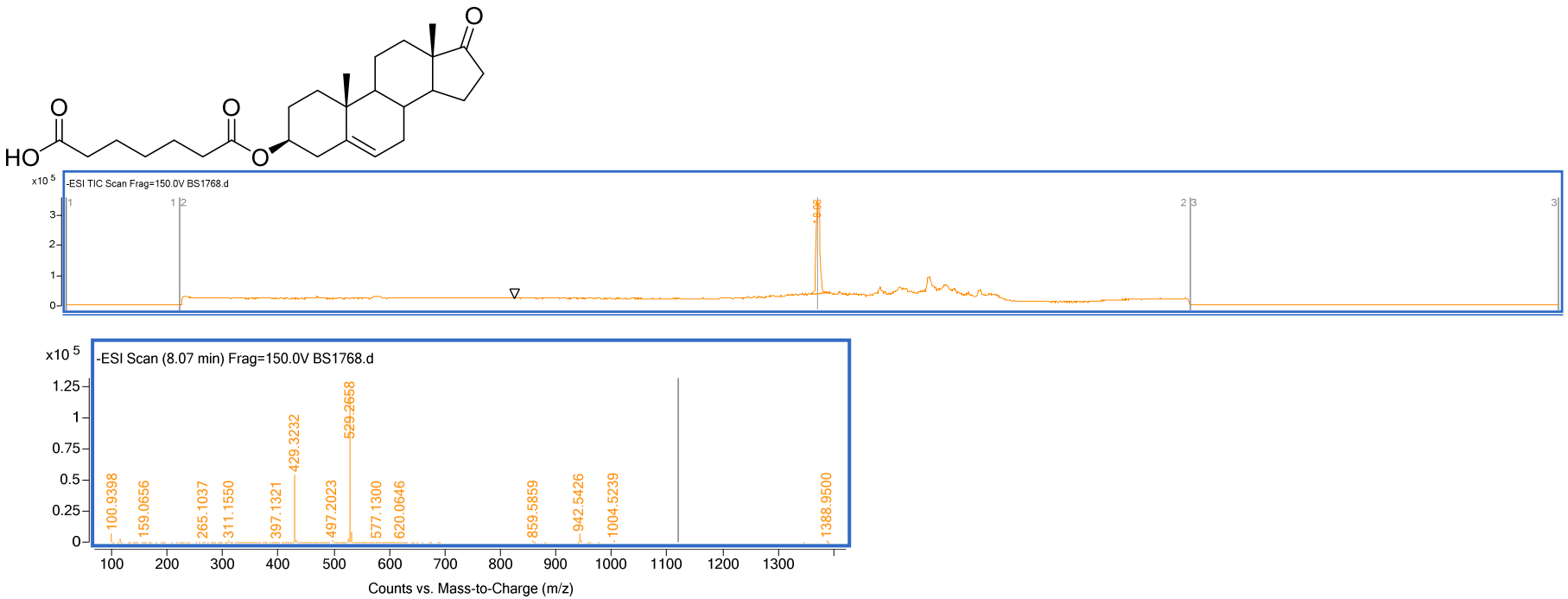
HO
O
O
O
O
x10 5
-ESI TIC Scan Frag=150.0V BS1768.d
-ESI Scan (8.07 min) Frag=150.0V BS1768.d
100.9398
159.0656
265.1037
311.1550
397.1321
429.3232
497.2023
529.2658
577.1300
620.0646
859.5859
942.5426
1004.5239
1388.9500
Counts vs. Mass-to-Charge (m/z)

Compound 22:

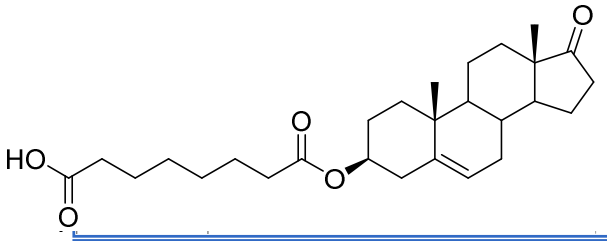
HO
O
O
O
O

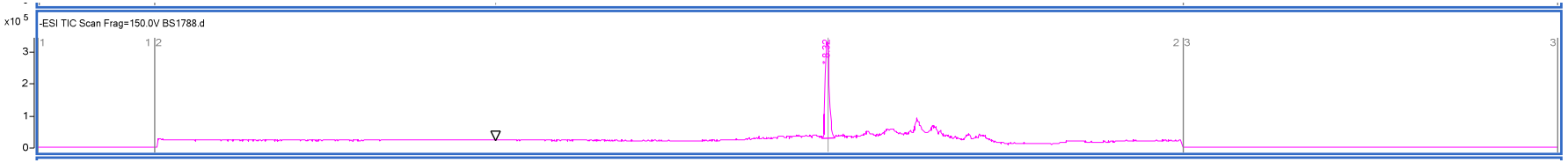
x10 5
-ESI TIC Scan Frag=150.0V BS1788.d
3
2
1
0

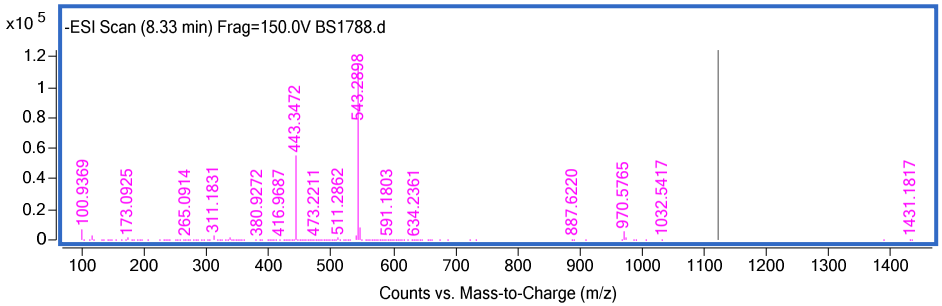
x10 5
-ESI Scan (8.33 min) Frag=150.0V BS1788.d
1.2
1
0.8
0.6
0.4
0.2
0
100.9369
173.0925
265.0914
311.1831
380.9272
416.9687
443.3472
473.2211
511.2862
543.2898
591.1803
634.2361
887.6220
970.5765
1032.5417
1431.1817
100
200
300
400
500
600
700
800
900
1000
1100
1200
1300
1400
Counts vs. Mass-to-Charge (m/z)

Compound 23:

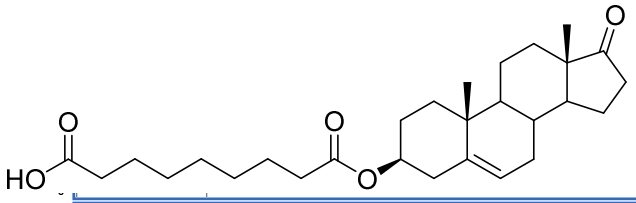
HO
O
O
O
O

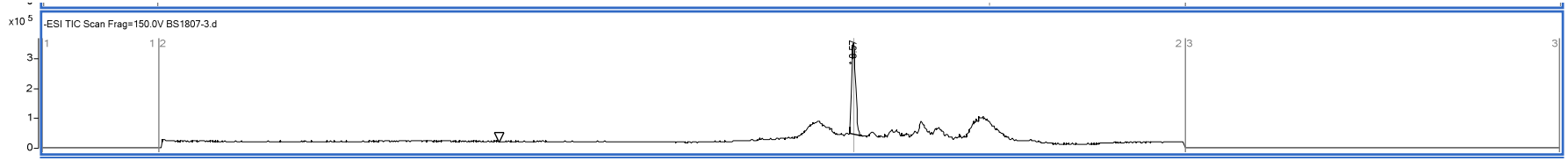
x10 5
-ESI TIC Scan Frag=150.0V BS1807-3.d
8.57

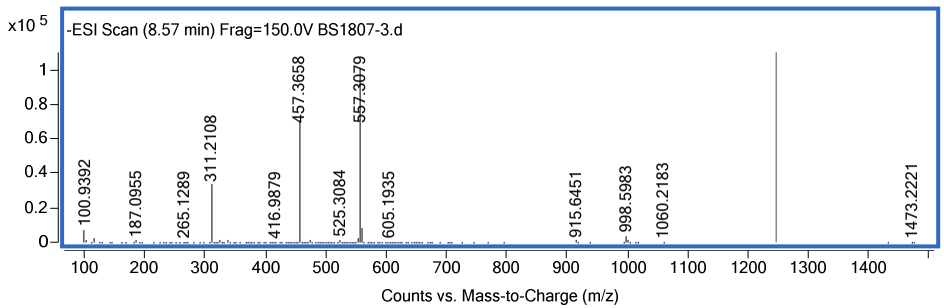
x10 5
-ESI Scan (8.57 min) Frag=150.0V BS1807-3.d
100.9392
187.0955
265.1289
311.2108
416.9879
457.3658
525.3084
557.3079
605.1935
915.6451
998.5983
1060.2183
1473.2221
Counts vs. Mass-to-Charge (m/z)

Compound 24:

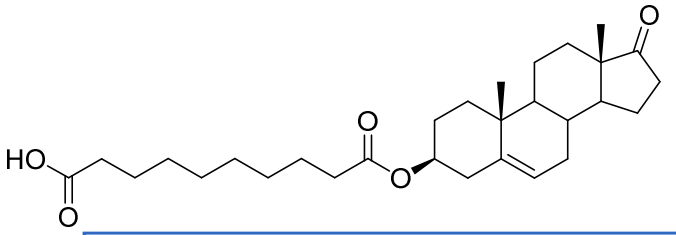
HO
O
O
O
O

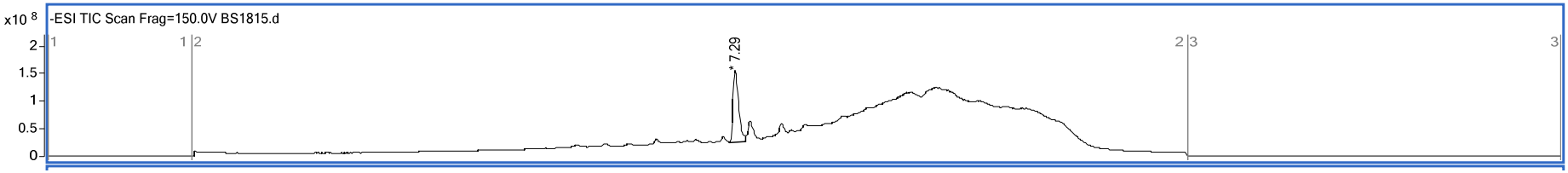
x10 8
-ESI TIC Scan Frag=150.0V BS1815.d
2
1.5
1
0.5
0
1
2
3
* 7.29

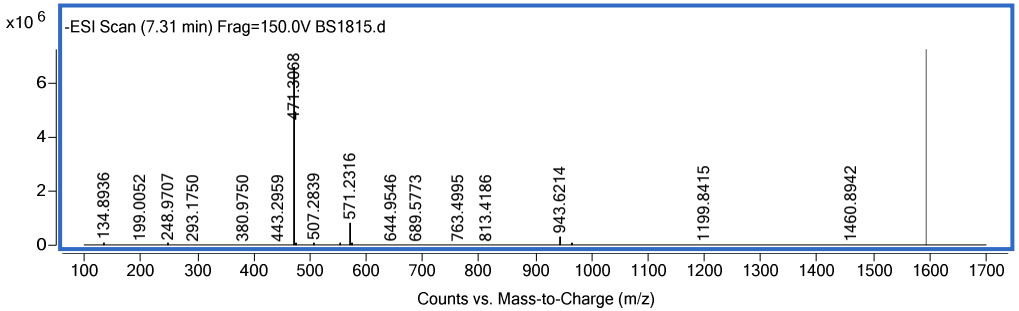
x10 6
-ESI Scan (7.31 min) Frag=150.0V BS1815.d
6
4
2
0
134.8936
199.0052
248.9707
293.1750
380.9750
443.2959
471.3968
507.2839
571.2316
644.9546
689.5773
763.4995
813.4186
943.6214
1199.8415
1460.8942
100
200
300
400
500
600
700
800
900
1000
1100
1200
1300
1400
1500
1600
1700
Counts vs. Mass-to-Charge (m/z)